A Heterogeneous Computational Model Reveals Temporal Hierarchy of Brain

Yaru Xu[1,†] (2024310105@link.tyut.edu.cn), Jing Wei[2,†] (20141032@sxufe.edu.cn), Yanqing Dong[1] (dongyanqing0078@link.tyut.edu.cn), Yan Niu[1] (niuyan@tyut.edu.cn), Jiayue Xue[2] (20241004@sxufe.edu.cn), Hao Guo[1] (feiyu_guo@sina.com), Yanli Yang[1,*] (yangyanli01@tyut.edu.cn), Jie Zhang[3,4,*] (jzhang080@gmail.com), Jie Xiang[1,*] (xiangjie@tyut.edu.cn)

[1] College of Computer Science and Technology (College of Data Science), Taiyuan University of Technology

[2] School of Information, Shanxi University of Finance and Economics

[3] Institute of Science and Technology for Brain-Inspired Intelligence, Fudan University

[4] Key Laboratory of Computational Neuroscience and Brain-Inspired Intelligence, Fudan University

[†] These authors contributed equally to this work, * Corresponding authors.

Abstract

Brain functional activity exhibits a distinct temporal hierarchy, characterized by the increase in intrinsic neural timescale (INT) from unimodal to transmodal cortices. However, existing large-scale brain network models struggle to accurately simulate this timescale hierarchy. This study developed a heterogeneous dynamic mean-field (hDMF) model by quantifying cortical microstructural differences using T1-weighted/T2-weighted (T1w/T2w) mapping. For model training, we proposed a novel multi-objective expectation maximization (MOEM) algorithm guided by bifurcation theory to achieve precise optimization in high-dimensional parameter spaces. Results demonstrated that the hDMF model significantly outperformed traditional models in fitting functional connectivity and metastable states, while successfully reproducing the gradient distribution of INT. Further application to ADNI clinical data revealed its ability to effectively simulate the abnormally elevated INT in Alzheimer's patients. In summary, this study provides a high-fidelity computational model for understanding the spatiotemporal brain dynamics and demonstrates potential clinical application value in biomarker exploration for neurodegenerative diseases.

Keywords: timescale hierarchy; parameter optimization; large-scale brain network model

Introduction

As a highly complex dynamical system, the spatiotemporal patterns of spontaneous brain activity arise from the interaction between the intrinsic dynamics of local circuits and their anatomical connections. Large-scale brain network models built on coupled brain regions with biophysically realistic properties can elucidate the intrinsic mechanisms underlying the functional organization of the brain and its dynamic evolution (Bassett et al., 2018). Recent studies have further revealed that the brain exhibits not only a hierarchical distribution in functional space, but also a distinct hierarchical structure in the temporal dynamics of neural activity. Transmodal association cortices can integrate information across extended time scales while maintaining stable functional states, whereas unimodal sensorimotor cortices respond rapidly to stimuli at short time scales (Gauthier et al., 2012; Hasson et al., 2008; Honey et al., 2012; Lerner et al., 2011; Stephens et al., 2013). Intrinsic neural timescales (INT) serve as a core metric for characterizing this temporal hierarchy (Chaudhuri et al., 2015; Golesorkhi et al., 2021; Murray et al., 2014; Wasmuht et al., 2018; Wolff et al., 2022). They have been identified across mammals at different evolutionary levels (Chaudhuri et al., 2015; Gao et al., 2020; Ito et al., 2020; Raut et al., 2020), revealing the temporal coding mechanisms of brain information processing. This makes INT an important research window for deciphering abnormal brain dynamics in neurological disorders (Wengler et al., 2020, 2024; Zhang et al., 2024b). Incorporating INT into brain dynamics modeling is crucial for enhancing its spatio-temporal dynamics characterization capabilities, thereby enabling a deeper understanding of the spatio-temporal evolution mechanisms underlying brain activity.

Early large-scale brain network models generally assumed that different brain regions share similar dynamics in local neural populations, thereby simplifying the complex biophysical modeling process. They typically fail to adequately account for the complex dynamic characteristics of brain activity, such as non-stationarity and state transitions. With the advancement of multimodal neuroimaging techniques, researchers have incorporated structural heterogeneity into brain network modeling, such as utilizing T1-weighted/T2-weighted (T1w/T2w) cortical gradients of myelination to reflect biophysical differences across brain regions (Chaudhuri et al., 2015; P. Wang et al., 2019). These groundbreaking studies provide a more systematic framework for understanding the dynamics of brain function. However, existing models still fail to fully capture the temporal diversity and information processing gradients of brain activity, particularly exhibiting significant shortcomings in simulating the INT (Chen et al., 2015; Cocchi et al., 2016; P. Wang et al., 2019). This limitation constrains the models' capacity for deep analysis of the spatio-temporal organization mechanisms in the real brain and their ability to dynamically reconstruct temporal abnormalities under pathological conditions. Therefore, there is a need to develop new modeling frameworks that integrate more refined dynamic constraints while preserving the advantages of modeling structural heterogeneity, in order to systematically capture the hierarchical features of the brain across temporal scales.

Existing heterogeneous brain network modeling accommodates complex regional differences by expanding the parameter space, but the automatic parameter search algorithms

In G. Boleda, I. Dautriche, M. Maldonado, C. Saldana and T. Torrent (Eds.), *Proceedings of the 48th Annual Conference of the Cognitive Science Society*

it relies on have inherent limitations. These algorithms focus on numerical fitting in high-dimensional spaces and lack targeted constraints on the dynamic principles of neural systems. While they can effectively fit functional connectivity (FC), they struggle to support the hierarchical structure of time scales that spontaneously emerges within the model (Castaldo et al., 2023; Monteverdi et al., 2023; Yang et al., 2024). As a nonlinear dynamical system, the dynamic switching and stability of brain functional activity are fundamentally regulated by bifurcation behavior. To overcome the limitations of existing methods, this study incorporates bifurcation theory into model parameter optimization. By constructing a dual-parameter bifurcation map of global coupling strength and local recurrent connectivity parameters, it precisely identifies the parameter region where the brain resides in a critical state. The system exhibits both stability and flexibility in this region, closely matching the dynamics of fluctuations near critical points observed in the real brain (Deco & Jirsa, 2012; S.-J. Wang & Zhou, 2022). Through qualitative dynamical analysis of critical regions, we propose an objective function constrained by multiple features, thereby providing a neurodynamical mechanism for constrained optimization in large-scale brain models.

This study incorporates the heterogeneity of myelin into large-scale brain network modeling, enabling precise characterization of the biophysical properties of brain regions. To optimize the model, this study innovatively proposes a multi-feature joint objective function constrained by neurodynamic mechanisms, achieving precise optimization in high-dimensional parameter spaces. This study makes three key contributions: First, the constraint mechanism based on bifurcation theory provides a neurodynamical rationale for model parameter optimization. Second, the multi-objective cost function translates complex neural activity features into quantifiable optimization metrics. Finally, the proposed modeling approach enhances the accuracy of functional connectivity fitting while enabling the spontaneous emergence of INT hierarchical gradient. Furthermore, extending this model to Alzheimer's disease successfully captures the characteristic pattern of abnormally elevated INT observed in patients. These findings provide new computational neuroscience insights into the functional dysregulation dynamics of neurodegenerative diseases.

Methods

Heterogeneous Dynamic Mean-field Model (hDMF)

The dynamic mean-field model (DMF) is an effective simplification of the detailed spike model (Deco et al., 2013), which can accurately and simply describe the relevant brain dynamics. It is obtained through coarse-grained approximation of the collective physiological discharge behavior of neuronal populations, without considering the detailed interactions between individual neurons. The behavior of interacting brain regions can be described by a set of coupled nonlinear differential equations:

$$\dot{S}_i = -\frac{S_i}{\tau_S} + r(1 - S_i)H(x_i) + \sigma\xi_i(t) \tag{1}$$

$$x_i = wJS_i + GJ\sum_j C_{ij}S_j + I \tag{2}$$

$$H(x_i) = \frac{ax_i - b}{1 - \exp(-d(ax_i - b))} \tag{3}$$

where, x_i , $H(x_i)$ and S_i represent the total input current, discharge rate, and average synaptic gating variables for each population in cortical region i, respectively. The connectivity strength of the structural connections scaled by the global coupling factor G. I represents the total excitatory subcortical input. The parameters are obtained from neurophysiological data to maintain the biophysical validity (Gordon et al., 2017). A comprehensive description of these parameters and the methodology for fitting large-scale dynamical models can be found in our previous study (Wei et al., 2022). The simulated neural activities S_i were fed to the Balloon–Windkessel hemodynamic model (Heinzle et al., 2016; Stephan et al., 2007), to simulate the BOLD signals for each brain region.

In the DMF, the recurrent connection strength w is assumed to be the same across different regions. Here, we relax the conditions of the model and parameterize the recurrent connection strength w using the T1w/T2w myelin map T_i. In this way, our heterogeneity model allows each region i had its own recurrent connection strength w_i. We refer to the resulting model as heterogeneous dynamic mean-field model (hMFM). Mye_i represents the value obtained by rescaling the T_i of the i-th brain region to the range from 0 to 1, the calculation formula is as follows:

$$Mye_i = \frac{T_i - \min\{T\}}{\max\{T\} - \min\{T\}} \tag{4}$$

$$w_i = w_0 + a_w Mye_i \tag{5}$$

where $i = 1, 2, ..., N$, where N represents the number of brain regions, w_0 represents the minimum value of the recurrent connection strength, and a_w is the scaling factor defining the hierarchical heterogeneity.

In order to emphasize the role of the cortical gradient approximated by the T1w/T2w myelin map in shaping the network dynamics, we have also constructed a random heterogeneous dynamic mean-field model (r_hDMF). We have used a random function to generate a 68×1 vector, where each element of the vector randomly takes values between 0 and 1 and serves as Mye_i of the i-th brain region. In this way, we simulate a cortical gradient without biological significance and explore the specific impact of the hierarchical heterogeneity of the cortical gradient on the network dynamics.

Multi-Objective Expectation Maximization (MOEM)

To enhance model accuracy and identify the optimal parameter combination for fitting empirical data, we conducted a bifurcation analysis on existing features used for model constraints, including the Pearson correlation of static FC, the

Kolmogorov–Smirnov (KS) distance of the functional connectivity dynamics (FCD) distribution (Kong et al., 2021), metastability(Cabral et al., 2011), synchrony(Cabral et al., 2011), the Kullback–Leibler (KL) divergence of PMS(Deco et al., 2019), and the Markov chain entropy of TPM(Deco et al., 2019). A thorough parameter space exploration was conducted by varying the global coupling factor G and the local coupling factor w. To optimize the model parameters by integrating multiple constraint features, we define the objective function as follows:

$$Goal = \sum f_i * goal_i \tag{6}$$

Where f_i is the weight of the i-th constraint feature, with $f_i > 0$, and $goal_i$ is the goodness-of-fit metric. A lower $Goal$ value indicates better model fit. To further validate the optimal parameter combinations, this study weighted the three indicators selected through bifurcation analysis, yielding seven potential objective functions:

$$\begin{cases} goal_1 = (1 - R_{FC}) + (1 - Meta) + KS \\ goal_2 = 2 * (1 - R_{FC}) + 0.5 * (1 - Meta) + 0.5 * KS \\ goal_3 = 0.5 * (1 - R_{FC}) + 2 * (1 - Meta) + 0.5 * KS \\ goal_4 = 0.5 * (1 - R_{FC}) + 0.5 * (1 - Meta) + 2 * KS \\ goal_5 = 2 * (1 - R_{FC}) + 2 * (1 - Meta) + 0.5 * KS \\ goal_6 = 2 * (1 - R_{FC}) + 0.5 * (1 - Meta) + 2 * KS \\ goal_7 = 0.5 * (1 - R_{FC}) + 2 * (1 - Meta) + 2 * KS \end{cases} \tag{7}$$

where R_{FC} denotes the Pearson correlation coefficient between the simulated and the empirical static FC matrix. KS represents the KS distance between the simulated and the empirical FCD matrix. $Meta$ indicates the metastable values of the simulated data.

The performance of the objective function is comprehensively evaluated through the following four parameters, with the sum of these factors constituting the model cost function. A lower value of the model cost function indicates better objective function performance, thereby enabling more reliable identification of the global optimum. Goodness of fit (GoF): The average value of each objective function across 30 simulations. Stability of goodness of fit (GoF-S): The standard deviation of each objective function across 30 simulations. Accuracy of parameter estimates (PEA): The average Euclidean distance between the 30 sets of parameter solutions found through objective function parameter optimization and the optimal solution identified via grid search. Stability of parameter estimates(PES): Evaluated by the average Euclidean distance among the 30 parameter solutions obtained for each objective function.

Intrinsic Neural Timescale (INT) Calculation

INT is calculated by assessing the autocorrelation amplitude of brain activity at rest, as shown in Figure 1. For each region i, the autocorrelation function (ACF) is computed as described by the formula:

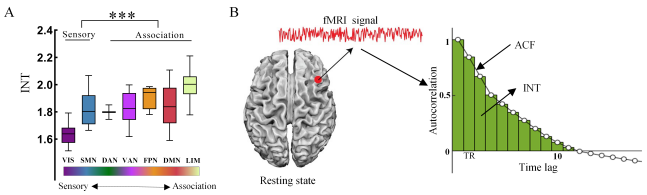

Figure 1: Definition and calculation of INT.(A) Group-average INT from the HCP dataset. (B) Calculation of INT based on resting-state functional magnetic resonance imaging (rs-fMRI) data.

$$ACF_k = \frac{\sum_{t=k+1}^{T}(y_t - \bar{y})(y_{t-k} - \bar{y})}{\sum_{t=1}^{T}(y_t - \bar{y})^2} \tag{8}$$

Here, k represents the time lag, T denotes the total number of time points, and y is the functional magnetic resonance imaging (fMRI) signal. The value of INT is approximated as the area under the ACF curve during the initial positive cycle (the sum of the green bar areas in Figure 1B). To adjust for differences in the temporal resolution of neural data, we multiply the sum of the obtained ACF values by the repetition time (TR) of the fMRI recording. The calculation method for INT is shown in the formula:

$$INT = TR \sum_{t=1}^{T} ACF_k \tag{9}$$

Dataset and Preprocessing

We used structural T1-weighted MRI, diffusion magnetic resonance imaging (dMRI), and resting-state functional MRI (rs-fMRI) from 45 subjects from the Human Connectome Project (HCP) Retest data release (Van Essen et al., 2013). Each scanning session included two resting-state runs that were acquired with 2 mm isotropic resolution with a TR of 720 ms and lasted for 1200 TRs. Details of the data collection can be found on the HCP website (http://www.humanconnectome.org/).

Data on neurodegenerative diseases were obtained from the Alzheimer's Disease Neuroimaging Initiative-3 (ADNI3; http://adni.loni.usc.edu/) encompassing subjects with Alzheimer's disease group (AD, 11 women and 14 men, mean age, 74.4±8.5 years), mild cognitive impairment group (MCI, 20 women and 18 men, mean age, 74.8±9.9 years), and cognitively normal group (CN, 25 women and 12 men, mean age, 76.5±7.2 years).

All MRI data were preprocessed using an HCP minimal preprocessing pipeline (Glasser et al., 2013). Intersubject alignment in the HCP dataset relied on multimodal areal-feature-based surface registration (MSMAll), which provides performance improvements over registration techniques based on geometric features only and reduces biases due to registration error in group-averaged datasets (Robinson et al., 2014).

The data preprocessing and feature extraction were carried out using the multimodal automated processing pipeline de-

veloped in our previous work (Wei et al., 2022). For each participant, based on the Desikan Killiany (Desikan et al., 2006) segmentation template, a 68 × 68 structural connectivity (SC) matrix was obtained. The weight of this matrix was generated by correcting the number of fiber bundles in the pairwise brain regions according to the surface area of the brain regions. The anatomical hierarchy was measured by the T1w/T2w maps released by the HCP. No further preprocessing was performed other than averaging the T1w/T2w values within each anatomical region of interest (ROI). Group-averaged T1w/T2w values were computed by averaging the data from all subjects.

For functional data, the BOLD signals of 68 brain regions are extracted based on the Desikan Killiany segmentation template. The fMRI data are averaged within each brain region, a 68 × 68 FC matrix is computed for each subject based on the Pearson correlation coefficients between BOLD time series. For each participant, the FC within each window was calculated using the sliding time window method, with each sliding window having a length of 83 TR (59.76 s). The correlation between the FC matrices of each sliding window was measured using Pearson correlation, generating a 1118 × 1118 FCD matrix.

In addition, we assigned 68 cortical regions to one of the 7 resting-state networks (RSNs) defined in Yeo et al (Yeo et al., 2011) by evaluating the area of overlap of the cortical surface. These 7 networks are named as follows: the frontoparietal control network (FPN), default mode network (DMN), limbic network (LIM), dorsal attention network (DAN), salience/ventral attention network (VAN), somatomotor network (SMN), and visual network (VIS).

Results

Model Parameter Selection

Based on bifurcation analysis, we systematically validated the critical parameter I in the model (Figure 2). In the group-level model of the HCP dataset, constructing the bifurcation distribution in the $G - w$ two-dimensional parameter space revealed that the optimal match between empirical FC and simulated FC occurred in the subcritical bifurcation region when $I = 0.32$. At this point, the brain system simultaneously exhibits characteristics of stable spontaneous states and high discharge states, suggesting the system is near a critical state. In the validation of individual models within the HCP dataset, the vast majority of subjects demonstrated optimal FC fitting performance around $I = 0.32$, indicating that this parameter possesses cross-individual stability.

To validate the universality of this parameter, we repeated the bifurcation analysis on the independent ADNI dataset within the CN group. Results showed that the optimal match for FC in the CN population also occurred at $I = 0.32$.

Result of the Objective Function for Minimizing Multi-Feature Joint Constraints

To further determine the model constraint metrics, we performed $G - w$ bifurcation analysis on R_{FC}, KS, KL, ME,

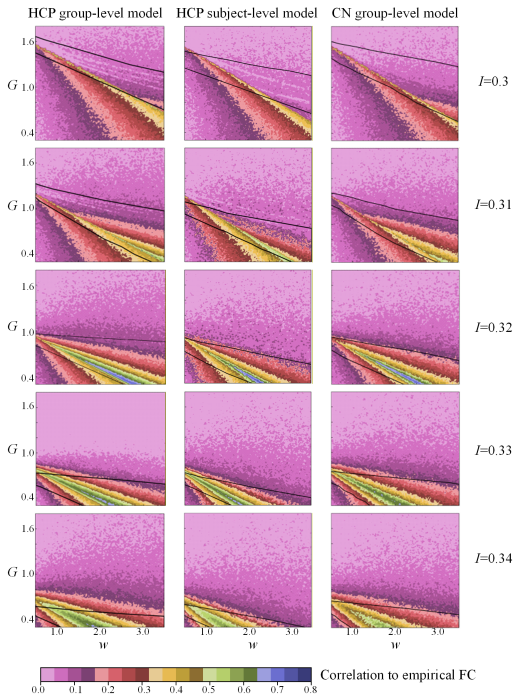

Figure 2: Based on bifurcation analysis, the model parameter I was determined for different datasets.

Metastability, and Synchrony separately, where the enclosed regions represent bifurcation zones. Figure 3A shows that bifurcation regions cover only a subset of $R_{FC} > 0.6$ areas while also including parameter combinations where $R_{FC} < 0.6$, indicating that R_{FC} alone cannot accurately constrain the model. The maximum fit for FCD is quantified by KS distance. In Figure 3B, regions where $KS < 0.2$ fully converge within the bifurcation region, suggesting that dynamic functional connectivity captures more nonlinear dynamic information [39]. Figure 3C-D quantify the fit between PMS and TPM using KL divergence and ME, respectively. When Kringelbach et al. (2020) constrained brain network models using these metrics, the corresponding values were remarkably low at 0.002 and 0.05 . However, in this study, PMS and TPM did not contribute significantly. Figure 3E shows that regions with $metastability > 0.02$ are entirely contained within bifurcation regions, validating metastability as an effective indicator of brain dynamic adaptability (Deco et al., 2015; Shine et al., 2019). Figure 3F demonstrates that the model exhibits no abnormally high synchrony under optimal parameters.

Based on the above results, we selected f R_{FC}, KS, and metastability as features for constructing the cost function. As shown in Table 1, the comparison results indicate that the objective function $goal_5$ outperforms other functions, yielding the best results. It exhibits significant advantages in GoF-S, PEA, and PES, indicating stronger robustness to outliers and higher stability of fitting results. Regarding the GoF, $goal_5$ ranks second only to $goal_4$ but still reflects high fitting accuracy. Therefore, we adopt $goal_5$ as the optimal objective

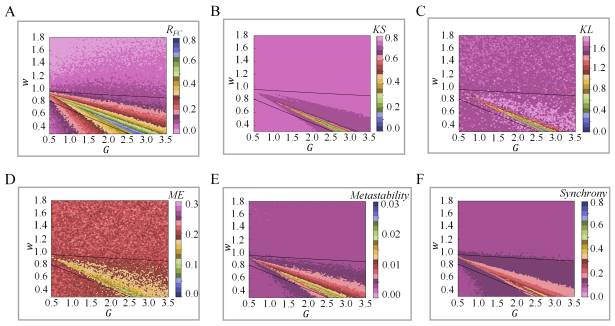

Figure 3: Bifurcation analysis identifies features for model constraints. (A) Pearson correlation coefficient R_{FC} for simulated and empirical FC. (B) Kolmogorov–Smirnov (KS) distance for simulated and empirical FCD. (C) Kullback-Leibler (KL) divergence of simulated ad empirical PMS. (D) Markov chain entropy (ME) for simulated and empirical TPM. (E) Metastable. (F) Synchrony.

function for the MOEM algorithm.

Table 1: Comparison of Objective Function.

Objective	GoF	GoF-S	PEA	PES	Cost
$goal_1$	0.4899	0.3264	0.3284	0.3471	1.4918
$goal_2$	0.4720	0.4341	**0.2087**	0.2662	1.3810
$goal_3$	0.9446	0.0805	0.3090	0.3429	1.6770
$goal_4$	**0.2235**	0.0015	0.2659	0.2807	0.7716
$goal_5$	0.3186	**0.0007**	0.2107	**0.2055**	**0.7355**
$goal_6$	0.3195	0.4031	0.2659	0.3146	1.3031
$goal_7$	0.3622	0.0245	0.2266	0.2748	0.8881

Evaluate the Performance of the hDMF

As shown in Figure 4, we compared the fitting performance of the traditional homogeneous DMF model, the structural heterogeneity hDMF model, and the random heterogeneity r_hDMF model under optimal parameters. At the FC level, the correlation between the FC matrix simulated by the hDMF model and the empirical FC matrix reached $r = 0.78$ ($p < 0.0001$, Figure 4A). This was significantly higher than both DMF ($r = 0.71$, $p < 0.0001$) and r_hDMF ($r = 0.69$, $p < 0.0001$, Figure 4B). The metastable drift of hDMF (0.009) was reduced by approximately 25% and 47% compared to DMF (0.012) and r_hDMF (0.017), respectively (Figure 4C). Regarding FCD, the hDMF model demonstrated the highest fit with empirical data, exhibiting a KS value of only 0.075, indicating that the hDMF model can authentically reproduce the dynamic functional connectivity patterns observed in empirical data (middle panel of Figure 4D). In contrast, the DMF model (left panel of Figure 4D, $KS = 0.504$) and r_hDMF model (right panel of Figure 4D, $KS = 0.368$) performed slightly worse, exhibiting greater discrepancies between their probability density function curves and the empirical data curve.

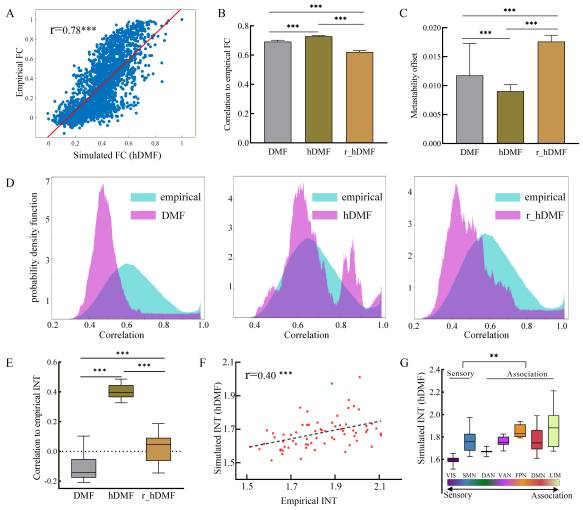

Figure 4: Performance Evaluation and Comparative Analysis of of hDMF. (A) Correlating between simulated and empirical FC of hDMF. Comparison of Different Models with empirical Data: (B) Pearson correlation coefficient for FC. (C) Metastable offset values. (D) Similarity of FCD distributions. (E) Pearson correlation coefficient for INT. (F) Correlation scatter plot between simulated INT from hDMF model and empirical INT data. (G) Hierarchical distribution of INT from hDMF.

In terms of functional time hierarchy, the results in Figure 4E indicate that the hDMF simulation results show significant correlation with the INT calculated from empirical data, whereas both DMF and r_hDMF perform poorly on this metric. Figure 4F illustrates the INT fitting between empirical data and the hDMF model ($r = 0.43$,$p < 0.001$), with data points exhibiting a distinct linear distribution trend. The hDMF successfully recreates the temporal gradient hierarchy across cortical regions, ranging from sensorimotor regions (VIS, SMN with shorter INT) to association regions (DMN, LIM with longer INT) (Figure 4G).

Robustness Analysis

As shown in Figure 5, we applied the model to the ADNI dataset to validate the robustness and generalization capability of the hDMF model across different datasets. Figure 5A demonstrates that despite differences in the magnitude of INT values among the CN, MCI, and AD groups, all groups exhibit a consistent pattern: relatively shorter INT values in unimodal regions and relatively longer INT values in cross-modal regions. The results in Figure 5B reveal that INT values across all subject groups increase along the structural gradient from sensorimotor regions to association areas. Compared to the CN group, the AD and MCI groups exhibit a general trend of increased average INT values across all brain regions.

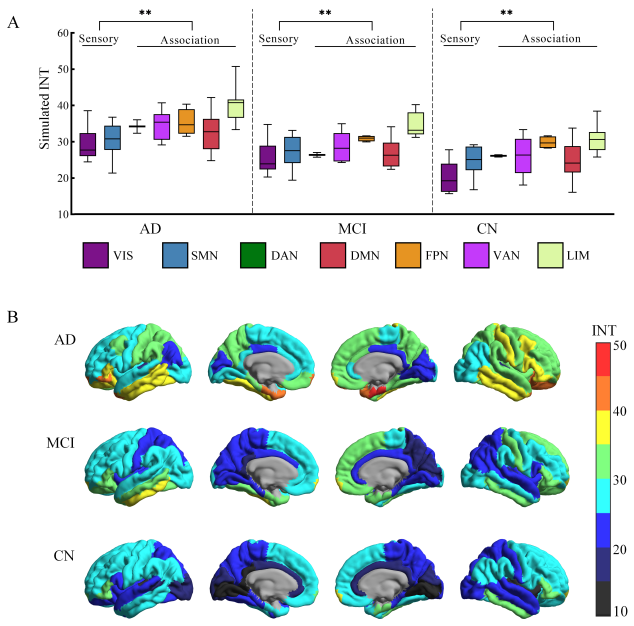

Figure 5: Robust validation of the hDMF in the ADNI dataset. (A) Group-average INT across different groups. (B) Group-average INT distribution across the entire brain.

Discussion

This study proposes a heterogeneous brain dynamics modeling approach based on multi-feature joint objective function optimization constrained by neurodynamic mechanisms, aiming to address the limitation of existing dynamic models in simulating the temporal hierarchical patterns of brain information processing. We introduce the MOEM based on bifurcation theory, whose core lies in guiding model parameter selection through steady-state analysis of the system. Unlike the black-box parameter scanning of traditional grid search, this approach defines the critical parameter range via bifurcation diagrams, providing a mechanism-driven optimization strategy. The brain must simultaneously maintain the stability of fundamental functional networks while responding to environmental changes through state transitions. This dual requirement aligns with bifurcation theory's description of parameter-critical systems possessing both robustness and flexibility (Beggs & Plenz, 2003). Model optimization based on bifurcation analysis shifts the parameter selection for brain network models from data-fitting to biologically grounded principles, providing a universal approach for constructing more interpretable brain network models.

The model constructed in this study demonstrates outstanding performance across multiple dimensional metrics. This balanced capability stems from the synergistic interaction between structural gradients and bifurcation theory. Structural gradients endow the model with spatial heterogeneity to align with functional differences among brain regions, while bifurcation theory ensures biological plausibility of dynamic properties by defining critical thresholds. This enables the model to simultaneously capture spatial connectivity patterns and temporal dynamic regularities(Friston, 2010). Mechanistically, association areas with low myelination exhibit slower neural signal integration due to weaker coupling strength (Demirtaş et al., 2019; Fotiadis et al., 2023), resulting in longer INT. Control experiments demonstrate that the random gradient model, lacking authentic structural gradient constraints, fails to fit INT, further underscoring the critical influence of cortical gradients on brain functional performance. Furthermore, research reveals that neurons in primary sensory cortices possess stronger reciprocal excitatory connections, with their excitatory-inhibitory balance favoring fast-response dynamics. This enables rapid processing of local information in these regions. In contrast, association cortices maintain information across temporal scales through extensive regulation by inhibitory interneurons, facilitating more complex cognitive tasks (Li & Wang, 2022). The heterogeneity in electrophysiological properties of excitatory and inhibitory neuronal populations across brain regions influences the distribution of local coupling factors. The gradient variation of w_i in this model essentially translates this anatomical heterogeneity in excitatory-inhibitory balance into a spatial distribution of dynamic parameters.

Finally, the consistency of parameter I=0.32 across the HCP and ADNI datasets in the CN group provides crucial evidence for the stability and generalization capability of the model. This cross-dataset parameter robustness suggests that this parameter may reflect the inherent requirement for maintaining a critical state in the healthy brain (Deco et al., 2013). Within the ADNI clinical data, hDMF captures the anomalous pattern of overall elevated INT in AD and MCI. This finding aligns with prior studies documenting temporal scale abnormalities in brain networks of AD patients (Zhang et al., 2024a), capturing a core dysfunction in structure-function coupling during neurodegenerative processes. The hDMF model constructed in this study combines structural gradients with bifurcation theory, providing a tool with both interpretability and generalization capability for analyzing brain functional hierarchies in normal and pathological states.

Conclusion

The core contribution of this study proposes a multi-objective expectation maximization algorithm constrained by neurodynamics to optimize a large-scale brain network model with structural gradient heterogeneity, achieving a breakthrough in reproducing the temporal hierarchical structure of brain function. The optimized core parameters demonstrate robust stability across individuals and datasets, enabling the model to precisely capture the abnormally elevated INT patterns observed in neurodegenerative disease patients. Consequently, this study endows brain network models with cross-scenario interpretability by bridging normal functional analysis and pathological mechanism exploration.

Acknowledgments

This work was supported by the following grants: Brain Science and Brain-like Intelligence Technology - National Science and Technology Major Project 2021ZD0200204 (Jie Zhang), the National Natural Science Foundation of China 62376184 (Jie Xiang), Central Guided Local Science and Technology Development Project YDZJSX20231A017 (Jie Xiang), the Humanities and Social Sciences Research Project of the Ministry of Education 25YJCZH280 (Jing Wei), and 24YJCZH366 (Jiayue Xue), Shanxi Provincial Application Basic Research Plan 202303021212166 (Jing Wei), and 202203021222095 (Jiayue Xue), and the Shanxi Province Graduate Research Innovation Project 2024KY194 (Yaru Xu).

References

Bassett, D. S., Zurn, P., & Gold, J. I. (2018). On the nature and use of models in network neuroscience. *Nature Reviews Neuroscience*, *19*(9), 566–578. https://doi.org/10.1038/s41583-018-0038-8

Beggs, J. M., & Plenz, D. (2003). Neuronal avalanches in neocortical circuits. *The Journal of Neuroscience*, *23*(35), 11167–11177. https://doi.org/10.1523/JNEUROSCI.23-35-11167.2003

Cabral, J., Hugues, E., Sporns, O., & Deco, G. (2011). Role of local network oscillations in resting-state functional connectivity. *NeuroImage*, *57*(1), 130–139. https://doi.org/10.1016/j.neuroimage.2011.04.010

Castaldo, F., Páscoa Dos Santos, F., Timms, R. C., Cabral, J., Vohryzek, J., Deco, G., Woolrich, M., Friston, K., Verschure, P., & Litvak, V. (2023). Multi-modal and multi-model interrogation of large-scale functional brain networks. *NeuroImage*, *277*, 120236. https://doi.org/10.1016/j.neuroimage.2023.120236

Chaudhuri, R., Knoblauch, K., Gariel, M.-A., Kennedy, H., & Wang, X.-J. (2015). A large-scale circuit mechanism for hierarchical dynamical processing in the primate cortex. *Neuron*, *88*(2), 419–431. https://doi.org/10.1016/j.neuron.2015.09.008

Chen, J., Hasson, U., & Honey, C. J. (2015). Processing timescales as an organizing principle for primate cortex. *Neuron*, *88*(2), 244–246. https://doi.org/10.1016/j.neuron.2015.10.010

Cocchi, L., Sale, M. V., L Gollo, L., Bell, P. T., Nguyen, V. T., Zalesky, A., Breakspear, M., & Mattingley, J. B. (2016). A hierarchy of timescales explains distinct effects of local inhibition of primary visual cortex and frontal eye fields. *eLife*, *5*, e15252. https://doi.org/10.7554/eLife.15252

Deco, G., Cruzat, J., Cabral, J., Tagliazucchi, E., Laufs, H., Logothetis, N. K., & Kringelbach, M. L. (2019). Awakening: Predicting external stimulation to force transitions between different brain states. *Proceedings of the National Academy of Sciences*, *116*(36), 18088–18097. https://doi.org/10.1073/pnas.1905534116

Deco, G., & Jirsa, V. K. (2012). Ongoing cortical activity at rest: Criticality, multistability, and ghost attractors. *The Journal of Neuroscience*, *32*(10), 3366–3375. https://doi.org/10.1523/JNEUROSCI.2523-11.2012

Deco, G., Ponce-Alvarez, A., Mantini, D., Romani, G. L., Hagmann, P., & Corbetta, M. (2013). Resting-state functional connectivity emerges from structurally and dynamically shaped slow linear fluctuations. *The Journal of Neuroscience*, *33*(27), 11239–11252. https://doi.org/10.1523/JNEUROSCI.1091-13.2013

Deco, G., Tononi, G., Boly, M., & Kringelbach, M. L. (2015). Rethinking segregation and integration: Contributions of whole-brain modelling. *Nature Reviews Neuroscience*, *16*(7), 430–439. https://doi.org/10.1038/nrn3963

Demirtaş, M., Burt, J. B., Helmer, M., Ji, J. L., Adkinson, B. D., Glasser, M. F., Van Essen, D. C., Sotiropoulos, S. N., Anticevic, A., & Murray, J. D. (2019). Hierarchical heterogeneity across human cortex shapes large-scale neural dynamics. *Neuron*, *101*(6), 1181–1194.e13. https://doi.org/10.1016/j.neuron.2019.01.017

Desikan, R. S., Ségonne, F., Fischl, B., Quinn, B. T., Dickerson, B. C., Blacker, D., Buckner, R. L., Dale, A. M., Maguire, R. P., Hyman, B. T., Albert, M. S., & Killiany, R. J. (2006). An automated labeling system for subdividing the human cerebral cortex on mri scans into gyral based regions of interest. *NeuroImage*, *31*(3), 968–980. https://doi.org/10.1016/j.neuroimage.2006.01.021

Fotiadis, P., Cieslak, M., He, X., Caciagli, L., Ouellet, M., Satterthwaite, T. D., Shinohara, R. T., & Bassett, D. S. (2023). Myelination and excitation-inhibition balance synergistically shape structure-function coupling across the human cortex. *Nature Communications*, *14*(1), 6115. https://doi.org/10.1038/s41467-023-41686-9

Friston, K. (2010). The free-energy principle: A unified brain theory? *Nature Reviews Neuroscience*, *11*(2), 127–138. https://doi.org/10.1038/nrn2787

Gao, R., van den Brink, R. L., Pfeffer, T., & Voytek, B. (2020). Neuronal timescales are functionally dynamic and shaped by cortical microarchitecture. *eLife*, *9*, e61277. https://doi.org/10.7554/eLife.61277

Gauthier, B., Eger, E., Hesselmann, G., Giraud, A.-L., & Kleinschmidt, A. (2012). Temporal tuning properties along the human ventral visual stream. *The Journal of Neuroscience*, *32*(41), 14433–14441. https://doi.org/10.1523/JNEUROSCI.2467-12.2012

Glasser, M. F., Sotiropoulos, S. N., Wilson, J. A., Coalson, T. S., Fischl, B., Andersson, J. L., Xu, J., Jbabdi, S., Webster, M., Polimeni, J. R., Van Essen, D. C., & Jenkinson, M. (2013). The minimal preprocessing pipelines for the Human Connectome Project. *NeuroImage*, *80*, 105–124. https://doi.org/10.1016/j.neuroimage.2013.04.127

Golesorkhi, M., Gomez-Pilar, J., Tumati, S., Fraser, M., & Northoff, G. (2021). Temporal hierarchy of intrinsic neural timescales converges with spatial core-periphery organiza-

tion. *Communications Biology*, *4*(1), 277. https://doi.org/10.1038/s42003-021-01785-z

Gordon, E. M., Laumann, T. O., Gilmore, A. W., Newbold, D. J., Greene, D. J., Berg, J. J., Ortega, M., Hoyt-Drazen, C., Gratton, C., Sun, H., Hampton, J. M., Coalson, R. S., Nguyen, A. L., McDermott, K. B., Shimony, J. S., Snyder, A. Z., Schlaggar, B. L., Petersen, S. E., Nelson, S. M., & Dosenbach, N. U. F. (2017). Precision functional mapping of individual human brains. *Neuron*, *95*(4), 791–807.e7. https://doi.org/10.1016/j.neuron.2017.07.011

Hasson, U., Yang, E., Vallines, I., Heeger, D. J., & Rubin, N. (2008). A hierarchy of temporal receptive windows in human cortex. *The Journal of Neuroscience*, *28*(10), 2539–2550. https://doi.org/10.1523/JNEUROSCI.5487-07.2008

Heinzle, J., Koopmans, P. J., den Ouden, H. E. M., Raman, S., & Stephan, K. E. (2016). A hemodynamic model for layered bold signals. *NeuroImage*, *125*, 556–570. https://doi.org/10.1016/j.neuroimage.2015.10.025

Honey, C. J., Thesen, T., Donner, T. H., Silbert, L. J., Carlson, C. E., Devinsky, O., Doyle, W. K., Rubin, N., Heeger, D. J., & Hasson, U. (2012). Slow cortical dynamics and the accumulation of information over long timescales. *Neuron*, *76*(2), 423–434. https://doi.org/10.1016/j.neuron.2012.08.011

Ito, T., Hearne, L. J., & Cole, M. W. (2020). A cortical hierarchy of localized and distributed processes revealed via dissociation of task activations, connectivity changes, and intrinsic timescales. *NeuroImage*, *221*, 117141. https://doi.org/10.1016/j.neuroimage.2020.117141

Kong, X., Kong, R., Orban, C., Wang, P., Zhang, S., Anderson, K., Holmes, A., Murray, J. D., Deco, G., van den Heuvel, M., & Yeo, B. T. T. (2021). Sensory-motor cortices shape functional connectivity dynamics in the human brain. *Nature Communications*, *12*(1), 6373. https://doi.org/10.1038/s41467-021-26704-y

Kringelbach, M. L., Cruzat, J., Cabral, J., Knudsen, G. M., Carhart-Harris, R., Whybrow, P. C., Logothetis, N. K., & Deco, G. (2020). Dynamic coupling of whole-brain neuronal and neurotransmitter systems. *Proceedings of the National Academy of Sciences*, *117*(17), 9566–9576. https://doi.org/10.1073/pnas.1921475117

Lerner, Y., Honey, C. J., Silbert, L. J., & Hasson, U. (2011). Topographic mapping of a hierarchy of temporal receptive windows using a narrated story. *The Journal of Neuroscience*, *31*(8), 2906–2915. https://doi.org/10.1523/JNEUROSCI.3684-10.2011

Li, S., & Wang, X.-J. (2022). Hierarchical timescales in the neocortex: Mathematical mechanism and biological insights. *Proceedings of the National Academy of Sciences*, *119*(6), e2110274119. https://doi.org/10.1073/pnas.2110274119

Monteverdi, A., Palesi, F., Schirner, M., Argentino, F., Merante, M., Redolfi, A., Conca, F., Mazzocchi, L., Cappa, S. F., Cotta Ramusino, M., Costa, A., Pichiecchio, A., Farina, L. M., Jirsa, V., Ritter, P., Gandini Wheeler-Kingshott, C. A. M., & D'Angelo, E. (2023). Virtual brain simulations reveal network-specific parameters in neurodegenerative dementias. *Frontiers in Aging Neuroscience*, *15*, 1204134. https://doi.org/10.3389/fnagi.2023.1204134

Murray, J. D., Bernacchia, A., Freedman, D. J., Romo, R., Wallis, J. D., Padoa-Schioppa, C., Pasternak, T., Seo, H., Lee, D., & Wang, X.-J. (2014). A hierarchy of intrinsic timescales across primate cortex. *Nature Neuroscience*, *17*(12), 1661–1663. https://doi.org/10.1038/nn.3862

Raut, R. V., Mitra, A., Marek, S., Ortega, M., Snyder, A. Z., Tanenbaum, A., Laumann, T. O., Dosenbach, N. U. F., & Raichle, M. E. (2020). Organization of propagated intrinsic brain activity in individual humans. *Cerebral Cortex*, *30*(3), 1716–1734. https://doi.org/10.1093/cercor/bhz198

Robinson, E. C., Jbabdi, S., Glasser, M. F., Andersson, J., Burgess, G. C., Harms, M. P., Smith, S. M., Van Essen, D. C., & Jenkinson, M. (2014). MSM: A new flexible framework for Multimodal Surface Matching. *NeuroImage*, *100*, 414–426. https://doi.org/10.1016/j.neuroimage.2014.05.069

Shine, J. M., Breakspear, M., Bell, P. T., Ehgoetz Martens, K. A., Shine, R., Koyejo, O., Sporns, O., & Poldrack, R. A. (2019). Human cognition involves the dynamic integration of neural activity and neuromodulatory systems. *Nature Neuroscience*, *22*(2), 289–296. https://doi.org/10.1038/s41593-018-0312-0

Stephan, K. E., Weiskopf, N., Drysdale, P. M., Robinson, P. A., & Friston, K. J. (2007). Comparing hemodynamic models with dcm. *NeuroImage*, *38*(3), 387–401. https://doi.org/10.1016/j.neuroimage.2007.07.040

Stephens, G. J., Honey, C. J., & Hasson, U. (2013). A place for time: The spatiotemporal structure of neural dynamics during natural audition. *Journal of Neurophysiology*, *110*(9), 2019–2026. https://doi.org/10.1152/jn.00268.2013

Van Essen, D. C., Smith, S. M., Barch, D. M., Behrens, T. E., Yacoub, E., & Ugurbil, K. (2013). The wu-minn human connectome project: An overview. *NeuroImage*, *80*, 62–79. https://doi.org/10.1016/j.neuroimage.2013.05.041

Wang, P., Kong, R., Kong, X., Liégeois, R., Orban, C., Deco, G., van den Heuvel, M. P., & Yeo, B. T. T. (2019). Inversion of a large-scale circuit model reveals a cortical hierarchy in the dynamic resting human brain. *Science Advances*, *5*(1), eaat7854. https://doi.org/10.1126/sciadv.aat7854

Wang, S.-J., & Zhou, C. (2022). Less is more: Wiring-economical modular networks support self-sustained firing-economical neural avalanches for efficient processing. *National Science Review*, *9*(3), nwab102. https://doi.org/10.1093/nsr/nwab102

Wasmuht, D. F., Spaak, E., Buschman, T. J., Miller, E. K., & Stokes, M. G. (2018). Intrinsic neuronal dynamics predict distinct functional roles during working memory. *Nature Communications*, *9*(1), 3499. https://doi.org/10.1038/s41467-018-05961-4

Wei, J., Wang, B., Yang, Y., Niu, Y., Yang, L., Guo, Y., & Xiang, J. (2022). Effects of virtual lesions on temporal dy-

namics in cortical networks based on personalized dynamic models. *NeuroImage*, *254*, 119087. https://doi.org/10.1016/j.neuroimage.2022.119087

Wengler, K., Goldberg, A. T., Chahine, G., & Horga, G. (2020). Distinct hierarchical alterations of intrinsic neural timescales account for different manifestations of psychosis. *eLife*, *9*, e56151. https://doi.org/10.7554/eLife.56151

Wengler, K., Goldberg, A. T., Chahine, G., & Horga, G. (2024). Altered hierarchical gradients of intrinsic neural timescales in mild cognitive impairment and alzheimer's disease. *The Journal of Neuroscience*, *44*(25), e2024232024. https://doi.org/10.1523/JNEUROSCI.2024-23.2024

Wolff, A., Berberian, N., Golesorkhi, M., Gomez-Pilar, J., Zilio, F., & Northoff, G. (2022). Intrinsic neural timescales: Temporal integration and segregation. *Trends in Cognitive Sciences*, *26*(2), 159–173. https://doi.org/10.1016/j.tics.2021.11.007

Yang, S., Zhou, Y., Peng, C., Meng, Y., Chen, H., Zhang, S., Kong, X., Kong, R., Yeo, B. T. T., Liao, W., & Zhang, Z. (2024). Macroscale intrinsic dynamics are associated with microcircuit function in focal and generalized epilepsies. *Communications Biology*, *7*(1), 145. https://doi.org/10.1038/s42003-024-05819-0

Yeo, B. T. T., Krienen, F. M., Sepulcre, J., Sabuncu, M. R., Lashkari, D., Hollinshead, M., Roffman, J. L., Smoller, J. W., Zöllei, L., Polimeni, J. R., Fischl, B., Liu, H., & Buckner, R. L. (2011). The organization of the human cerebral cortex estimated by intrinsic functional connectivity. *Journal of Neurophysiology*, *106*(3), 1125–1165. https://doi.org/10.1152/jn.00338.2011

Zhang, A., Wengler, K., Zhu, X., Horga, G., Goldberg, T. E., & Lee, S. (2024a). Altered hierarchical gradients of intrinsic neural timescales in mild cognitive impairment and Alzheimer's disease. *The Journal of Neuroscience*, *44*(25), e2024232024. https://doi.org/10.1523/JNEUROSCI.2024-23.2024

Zhang, A., Wengler, K., Zhu, X., Horga, G., Goldberg, T. E., & Lee, S. (2024b). Altered hierarchical gradients of intrinsic neural timescales in mild cognitive impairment and alzheimer's disease. *The Journal of Neuroscience*, *44*(25), e2024232024. https://doi.org/10.1523/JNEUROSCI.2024-23.2024